

Layered $\text{Ca}_{0.28}\text{MnO}_2 \cdot 0.5\text{H}_2\text{O}$ as a High Performance Cathode for Aqueous Zinc-Ion Battery

Tianjiang Sun, Qingshun Nian, Shibing Zheng, Jinqiang Shi, and Zhanliang Tao*

Aqueous zinc-ion batteries are promising candidates for grid-scale energy storage because of their intrinsic safety, low cost, and high energy intensity. However, lack of suitable cathode materials with both excellent rate performance and cycling stability hinders further practical application of aqueous zinc-ion batteries. Here, a nanoflake-self-assembled nanorod structure of $\text{Ca}_{0.28}\text{MnO}_2 \cdot 0.5\text{H}_2\text{O}$ as Zn-insertion cathode material is designed. The $\text{Ca}_{0.28}\text{MnO}_2 \cdot 0.5\text{H}_2\text{O}$ exhibits a reversible capacity of 298 mAh g^{-1} at 175 mA g^{-1} and long-term cycling stability over 5000 cycles with no obvious capacity fading, which indicates that the per-insertion of Ca ions and water can significantly improve reversible insertion/extraction stability of Zn^{2+} in Mn-based layered type material. Further, its charge storage mechanism, especially hydrogen ions, is elucidated. A comprehensive study suggests that the intercalation of hydrogen ions in the first discharge plat is controlled by both pH value and type of anion of electrolyte. Further, it can stabilize the $\text{Ca}_{0.28}\text{MnO}_2 \cdot 0.5\text{H}_2\text{O}$ cathode and facilitate the following insertion of Zn^{2+} in $1 \text{ M ZnSO}_4/0.1 \text{ M MnSO}_4$ electrolyte. This work can enlighten and promote the development of high-performance rechargeable aqueous zinc-ion batteries.

include Prussian blue analogs, vanadium-based materials, and manganese-based materials.^[3] Among the various types of cathode materials, MnO_2 , with higher capacity ($>250 \text{ mAh g}^{-1}$), higher voltage (1.3–1.5 V), and various crystallographic polymorphs (α -, β -, γ -, δ -, λ -, and ε -type), is widely researched in ZIBs.^[4,5] Especially, layered-type $\delta\text{-MnO}_2$ (birnessite-type manganese oxides) exhibits a large inter-spacing channel ($\approx 0.7 \text{ nm}$),^[6,7] which is much more suitable for fast and reversible (de-)intercalation of Zn ions. Unfortunately, the $\text{Zn}/\delta\text{-MnO}_2$ battery system suffers from bad electrochemical performance, including significant capacity fading and poor rate capability. According to literatures, the $\delta\text{-MnO}_2$ exists serious structural transformation during cycling, as well as the dissolution of Mn, which are the key reasons for the poor cycling stability of $\text{Zn}/\delta\text{-MnO}_2$ battery.^[6,8] Moreover, the strong electrostatic interaction

1. Introduction

Aqueous Zn-ion batteries (ZIBs) are receiving increasing attention owing to their unique advantages of Zn anode, which include high theoretical specific capacity (820 mAh g^{-1}), relatively low redox potential (-0.76 V vs standard hydrogen electrode), and appropriate stability in mild acidic electrolyte.^[1] In addition, compared with aqueous alkali metal ion battery (Li^+ , Na^+ , K^+), the Zn anode of aqueous ZIBs involves a two-electron transfer during charge/discharge process to ensure high energy density (5851 mAh mL^{-1}) and a large storage capacity.^[2] Therefore, aqueous ZIBs promise to be the best candidate for aqueous metal ion battery in grid-scale electrochemical energy storage.


However, a lack of robust cathode materials remains a fundamental bottleneck to further promoting ZIBs practical application. The reported cathode materials for aqueous ZIBs mainly

between Zn^{2+} and host materials leads to the terrible rate capability of $\text{Zn}/\delta\text{-MnO}_2$ battery.^[9]

Liu et al. find that extra addition of Mn^{2+} into the electrolyte is a good strategy to inhibit the dissolution of Mn^{2+} from Mn^{3+} disproportionation.^[10] In addition, it is a common strategy in vanadium-based materials to introduce metal ions (Ca^{2+} , Zn^{2+} , Na^+ , Mg^{2+}) and crystalline water as pillars between interlayers to stabilize the layered structure.^[11] These cathode materials have efficient electrochemical performance due to strong ionic bonds between metal ions and oxygen atoms in lattice, which effectively hinder interlayer slip and structure collapse. For example, Nazar et al. report $\text{Zn}_{0.25}\text{V}_2\text{O}_5 \cdot n\text{H}_2\text{O}$ as cathode material for aqueous ZIBs, which shows high capacity (300 mAh g^{-1} at 0.05 A g^{-1}), long cycling life (1000 cycles at 4.5 A g^{-1}), and excellent rate performance.^[12] Similar to vanadium-based materials, layered manganese oxides can be studied to improve the electrochemical performance. So far, however, there have been few efforts to explore layered manganese oxides with pillar structure in ZIBs system, which is worth trying.

In addition, the aqueous Zn/MnO_2 battery exhibits complicated energy storage mechanism. It is generally believed that the Zn^{2+} and H^+ ions insert into $\delta\text{-MnO}_2$ by two steps in $\text{ZnSO}_4/\text{MnSO}_4$ electrolyte.^[5,13] In the first step, the H^+ ions insert into $\delta\text{-MnO}_2$ and form MnOOH and $\text{ZnSO}_4 \cdot 3\text{Zn}(\text{OH})_2 \cdot x\text{H}_2\text{O}$, then the Zn^{2+} ions intercalate into $\delta\text{-MnO}_2$ and form spinel ZnMn_2O_4 in the following step.^[14] Moreover, Pan et al. also confirm the joint charge storage of Zn^{2+} and H^+ ions of $\delta\text{-MnO}_2$

T. Sun, Q. Nian, Dr. S. Zheng, J. Shi, Prof. Z. Tao
 Key Laboratory of Advanced Energy Materials Chemistry
 (Ministry of Education)
 College of Chemistry
 Nankai University
 Tianjin 300071, P. R. China
 E-mail: taozhl@nankai.edu.cn

 The ORCID identification number(s) for the author(s) of this article can be found under <https://doi.org/10.1002/smll.202000597>.

DOI: 10.1002/smll.202000597

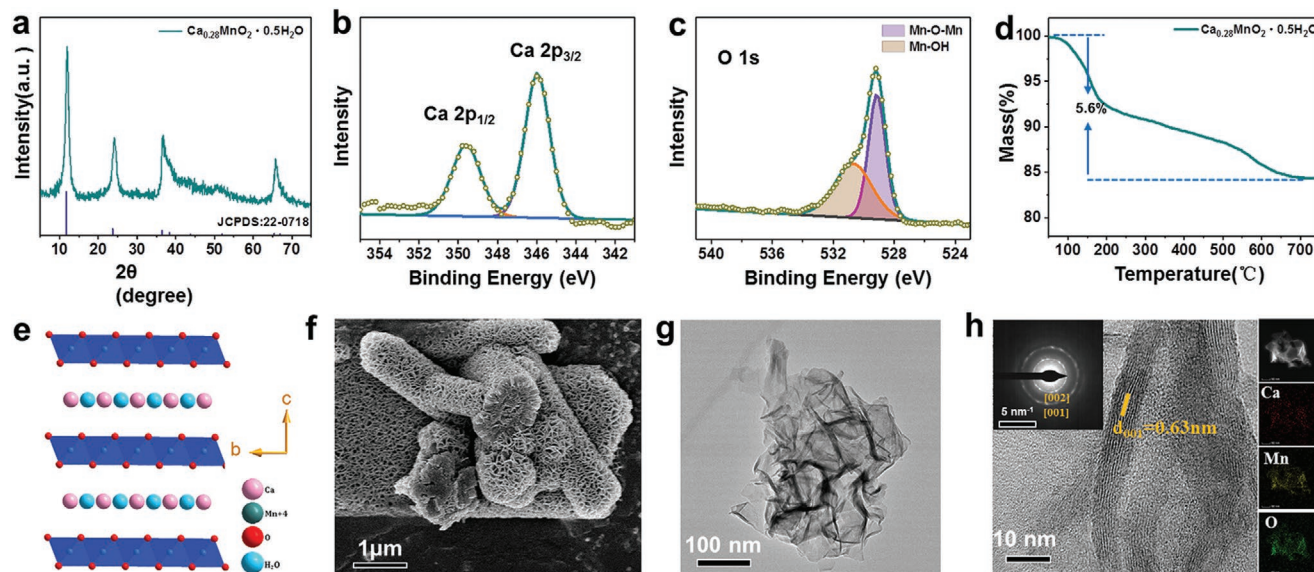


Figure 1. a) XRD pattern of CaMnO. b) XPS of Ca 2p; c) O 1s. d) TGA curve of the as-prepared CaMnO sample from 30 to 800 °C. e) Structural illustration of the as-prepared CaMnO. f) SEM; g) TEM; h) HRTEM, SAED, and EDX of CaMnO.

in 1 M Zn(TFSI)₂/0.1 M Mn(TFSI)₂. However, Kheawhom et al. suggest that only Zn²⁺ ions insert into δ -MnO₂ and transform into δ -ZnMnO₂ in 0.5 M ZnSO₄ electrolyte.^[15] Additionally, Kang et al. study the mechanism of Zn²⁺ ions intercalation in α -MnO₂, the formation of ZnMn₂O₄ clearly confirms the insertion of Zn²⁺ into α -MnO₂ in 0.5 M Zn(NO₃)₂ electrolyte.^[16] There is no doubt that the Zn²⁺ ions can be reversibly inserted/extracted in MnO₂. However, the insertion of H⁺ ions in MnO₂ still remains controversial, and is very sensitive to the local electrolyte. The lack of detailed study of H⁺ ions' storage mechanism has limited the development of more efficient and reliable electrode materials for practical applications.

Here, we design a novel aqueous ZIBs cathode material, which used Ca ion and water as pillars pre-insert into layered δ -MnO₂, namely, Ca_{0.28}MnO₂·0.5H₂O (CaMnO), and shows an excellent electrochemical performance in 1 M ZnSO₄/0.1 M MnSO₄ electrolyte. The CaMnO delivers an ultralong cycling life of 5000 cycles with no obvious capacity fading. Even at a high current density of 3.5 A g⁻¹, the CaMnO still maintains a large discharge capacity of 124 mAh g⁻¹. We also demonstrate that the H⁺ ions storage is controlled by pH value and type of anion of the electrolyte, and it can significantly improve the electrochemical performance of the layered CaMnO cathode.

2. Results and Discussion

The birnessite-type CaMnO is synthesized by a simple one-step hydrothermal method. The as-obtained sample is characterized by X-ray diffraction (XRD). As shown in the XRD pattern (Figure 1a), the (001) and (002) peaks corresponding to the layered structure (JCPDS No. 80-1098) of CaMnO, and no obvious impurity peaks are detected. It is noted that the (001) peak of CaMnO shifts to lower degree compared to δ -MnO₂ (Figure S1, Supporting Information). It may originate from the big volume effect of hydrate Ca ion, thus causes the layer

expansion of δ -MnO₂. The detailed elements' composition of Ca, O, and Mn is investigated through X-ray photoelectron spectroscopy (XPS). As shown in Figure 1b, the presence of Ca is confirmed by the appearance of a peak around 346.0 eV (corresponding to Ca 2p_{3/2}) and 349.6 eV (corresponding to Ca 2p_{1/2}),^[17] and the ratio of Ca/Mn was calculated to be 0.24. The O 1s spectrum (Figure 1c) shows that three obvious peaks with binding energy of 529.1, 530.7, and 532.4 eV, corresponding to Mn–O–Mn bond, Mn–O–H bond, and H–O–H bond, respectively.^[7] The presence of Mn–O–H bond and H–O–H bond indicates that a significant amount of crystal water has been intercalated into CaMnO. In addition, the detailed composition of Mn element is investigated by Mn 2p spectrum. As shown in Figure S2 in the Supporting Information, about 66.2% Mn⁴⁺ and 33.8% Mn³⁺ exist in as-prepared CaMnO. The inductively couple plasma optical emission spectrometry (ICP-OES) result confirms the atomic ratio of Ca:Mn = 0.28:1. Further, as displayed in Figure 1d, the thermogravimetric analysis (TGA) indicates that the number of lattice water in the CaMnO is 0.5. Therefore, the molecular formula of the CaMnO can be expressed as Ca_{0.28}MnO₂·0.5H₂O. A schematic structure of CaMnO is displayed in Figure 1e, the Ca ions and water molecules are inserted between the interlayer, which is beneficial for stabilizing the layered structure. As shown in Figure 1f,g and Figures S3 and S4 in the Supporting Information, the scanning electron microscopy (SEM) and transmission electron microscopy (TEM) images indicate that the CaMnO is composed of nanorods and nanospheres, formed by uniform interconnected nanoflakes. The nanopography of CaMnO provides abundant contact interfaces between electrode and electrolyte, which can shorten the Zn²⁺ ion diffusion channel and enable fast reaction kinetics. The high-resolution TEM (HRTEM) image (Figure 1h) shows clear lattice fringes with a spacing of 0.63 nm, corresponding to the characteristic (001) plane of CaMnO. In addition, the (001) and (002) planes can be clearly observed in the selected area

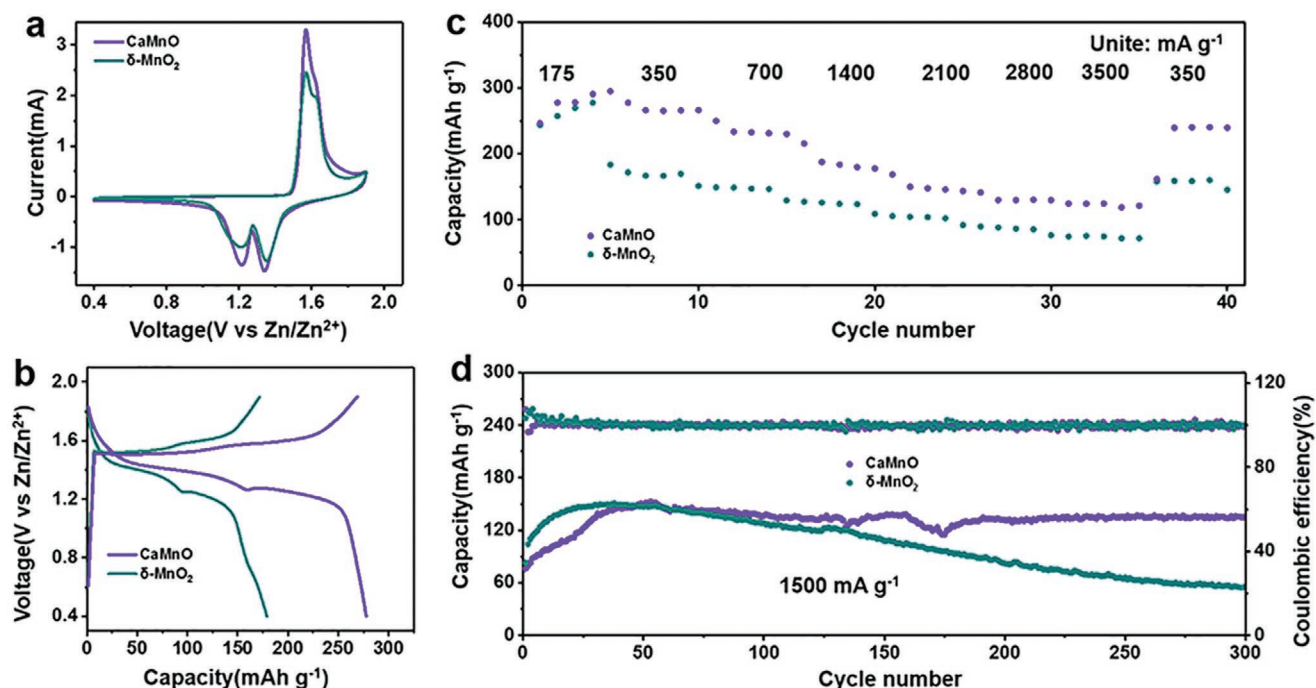


Figure 2. a) CV curves of CaMnO and δ -MnO₂ at 0.5 mV s⁻¹ (in the second cycle). b) Charge-discharge curves of CaMnO and δ -MnO₂ at 350 mA g⁻¹ (in the fifth cycle). c) Rate performance of CaMnO and δ -MnO₂. d) Cycling stability of CaMnO and δ -MnO₂ at 1500 mA g⁻¹.

electron diffraction (SAED) ring pattern. The energy-dispersive spectroscopy (EDX) elemental mapping images show that the Ca, Mn, and O elements are evenly distributed in CaMnO nanoflakes. The Raman spectrum of CaMnO in Figure S5a in the Supporting Information shows the characteristic peak at 252 cm⁻¹ corresponding to stretching vibration of Ca–O, which cannot be observed in δ -MnO₂ (Figure S5b, Supporting Information).^[18] The Raman spectrum further confirms that the CaMnO sample is successfully synthesized. To confirm the stability of Ca²⁺ in CaMnO, the XRD patterns of CaMnO with different soaking times in 1 M ZnSO₄/0.1 M MnSO₄ electrolyte are collected. Figure S6 in the Supporting Information shows that the (001) peak can be clearly observed even soaking after 2 weeks, which indicates significant stability of Ca ions in CaMnO.

To investigate the effect of pre-insertion of Ca ions and water in δ -MnO₂, the electrochemical performance of CaMnO and δ -MnO₂ electrodes is tested in coin cells using Zn foil anode, glass fiber separator, and 1 M ZnSO₄/0.1 M MnSO₄ electrolyte. The addition of manganese salt in electrolyte inhibits the Mn²⁺ dissolution. The cyclic voltammetry (CV) plots of CaMnO and δ -MnO₂ electrodes are collected within the voltage window of 0.4–1.9 V versus Zn/Zn²⁺ at 0.5 mV s⁻¹. The five cycle CV curves of CaMnO and δ -MnO₂ (Figure S7a,b, Supporting Information) are collected at 0.5 mV s⁻¹. The difference between the first cycle and sequent four-turn cycles indicates that the first cycle is irreversible. Moreover, the increasing response current represents a pre-activation process of fresh CaMnO and δ -MnO₂. Compared with δ -MnO₂, the CaMnO electrode exhibits greater response current, corresponding to the higher capacity (Figure 2a). The galvanostatic charge-discharge curves of CaMnO and δ -MnO₂ under a current density of 350 mA g⁻¹

are shown in Figure 2b. The plateaus of charge/discharge can be obviously discerned, and the CaMnO exhibits a high discharge specific capacity of 277.7 mAh g⁻¹ at 350 mA g⁻¹, while the δ -MnO₂ only has a discharge specific capacity of 179 mAh g⁻¹. It is worth noting that the overpotential of CaMnO is lower than δ -MnO₂, which indicates rapid reaction kinetics of CaMnO. As shown in Figure S8 in the Supporting Information, the CaMnO electrode delivers a higher discharge voltage of \approx 1.5 V versus Zn/Zn²⁺ and specific capacity of 298 mAh g⁻¹ at 175 mA g⁻¹, which is close to the theoretical specific capacity of δ -MnO₂. Moreover, CaMnO electrode possesses an excellent rate performance than δ -MnO₂, and still obtains a high discharge specific capacity of 124.5 mAh g⁻¹ at considerably high current density of 3500 mA g⁻¹ (Figure 2c). As displayed in Figure 2d, both CaMnO and δ -MnO₂ undergo an activation process in the first 50 cycles. The CaMnO electrode maintains a high discharge specific capacity of 135 mAh g⁻¹ at 1500 mA g⁻¹, while the δ -MnO₂ electrode shows the rapid capacity fading with only 54.9 mAh g⁻¹ after 300 cycles. The impressive capacity retention of CaMnO electrode demonstrates that the incorporation of Ca ions and water in layered δ -MnO₂ would maintain the structure stability, thus sustain a more stable cycle life in aqueous ZIBs.

To further understand the intrinsic reasons of excellent rate performance and long-term cycling stability of CaMnO, we analyze the electrochemical kinetics by the CV curves at different scan rates. As shown in Figure 3a, two discharge peaks and one charge peak are obviously observed, and these peaks show the same shape. The relationship of scan rate and peak current obeys the following equation^[19]

$$i = av^b \quad (1)$$

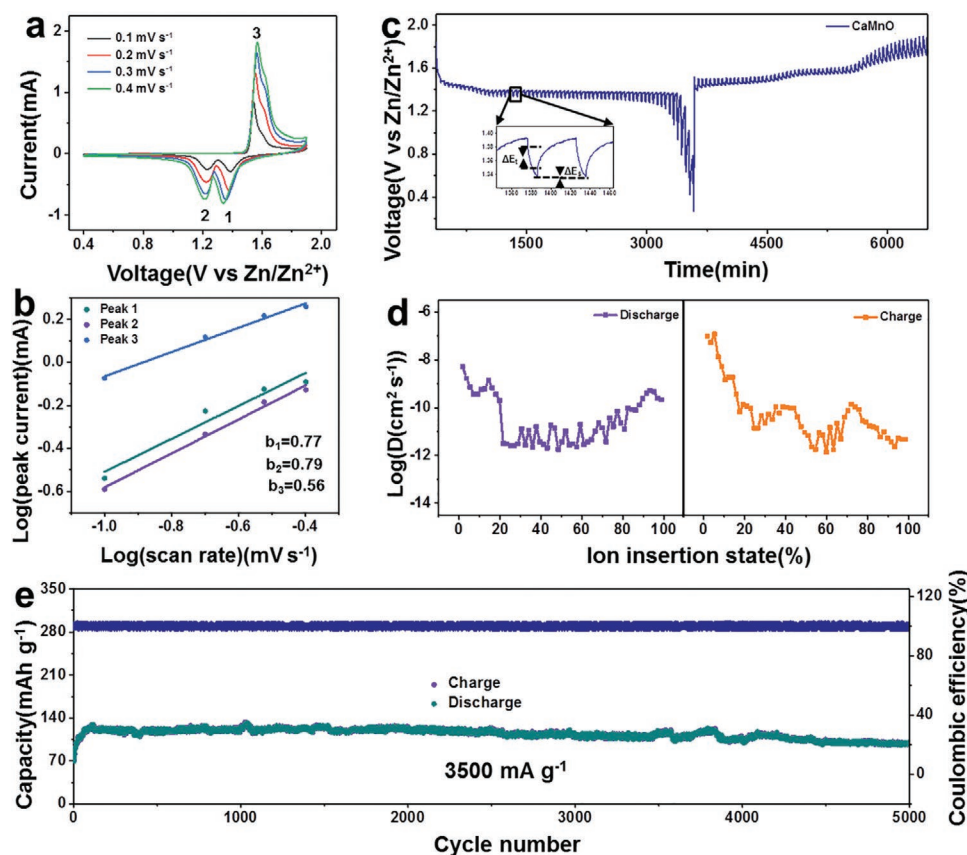


Figure 3. a) CV curves of CaMnO at different scan rates. b) Log(peak current) versus Log(scan rate) plots of three peaks in CV curves. c) The charge/discharge GITT profiles of the Zn//CaMnO. d) Diffusion coefficients calculated from the GITT potential profiles for CaMnO (in terms of charge states in the second cycle). e) Cycling stability of CaMnO at 3500 mA g⁻¹.

where i refers to the peak current (mA), v refers to the scan rate (mV s⁻¹), and a and b are adjustable parameters. The b value reflects the charge storage mechanism, when the $b = 1$, corresponding to surface-controlled process, while $b = 0.5$, suggesting a diffusion-controlled process. The calculated values of b for peak 1, peak 2, and peak 3 are 0.77, 0.79, and 0.56, respectively, which imply that the solid-state ions diffusion is the rate-limiting step for charge storage (Figure 3b). Furthermore, the capacitive contributions of CaMnO electrode at different scan rates are further calculated by simple CV method. The results are summarized in Figure S9 in the Supporting Information, the capacitive contribution is 66% at 0.1 mV s⁻¹ and gradually increasing to 84% at 0.4 mV s⁻¹, indicates fast reaction kinetics of CaMnO electrode in aqueous ZIBs. On the other hand, the galvanostatic intermittent titration technique (GITT) is applied to estimate the ion diffusion coefficient in CaMnO electrode. The calculation method is according to the following equation:^[20]

$$D = \frac{4}{\pi \tau} \left(\frac{n_m V_m}{S} \right)^2 \left(\frac{\Delta E_s}{\Delta E_t} \right)^2 \quad (2)$$

where n_m , V_m , and S are the moles of active materials, molar volume, and contact area between electrode and electrolyte, respectively. τ is the time duration of the pulse. ΔE_s and ΔE_t

are the change of quasi-equilibrium voltage and battery voltage, respectively. As shown in detailed drawing of Figure 3c, the system experiences a pulse of 3 mA for 10 min after a rest of 40 min. The calculation results are displayed in Figure 3d, the ions diffusion coefficients of CaMnO at discharge state are ranging from 2.6×10^{-11} to 5.3×10^{-9} cm² s⁻¹, indicate the fast ion diffusion kinetics. The ions diffusion coefficients also can be calculated by reported CV method. As shown in Figure S10 in the Supporting Information, the diffusion coefficients are calculated to be 2.9×10^{-9} , 2.6×10^{-9} , and 1.0×10^{-8} cm² s⁻¹ for peak 1, peak 2, and peak 3, which matched well with GITT. This property can be further confirmed by the electrochemical impedance spectroscopy (EIS) analysis, the Zn//CaMnO and Zn// δ -MnO₂ cells are rested for 30 min to the interfacial equilibrium. As shown in Figure S11a in the Supporting Information, the two systems have big semicircle, which indicates the quite high interfacial charge transfer resistances for initial cathodes. Then, with five-cycle activation process, the interfacial charge transfer resistances for CaMnO and δ -MnO₂ rapidly decrease (Figure S11b, Supporting Information). Note that, the interfacial charge transfer resistances of CaMnO are more lower than δ -MnO₂, which is likely benefited from the lowered Zn-adsorption energy by Ca ions pre-inserted in δ -MnO₂.^[17] Benefited by the good rate performance, the long-term stability of CaMnO is further tested at higher current density.

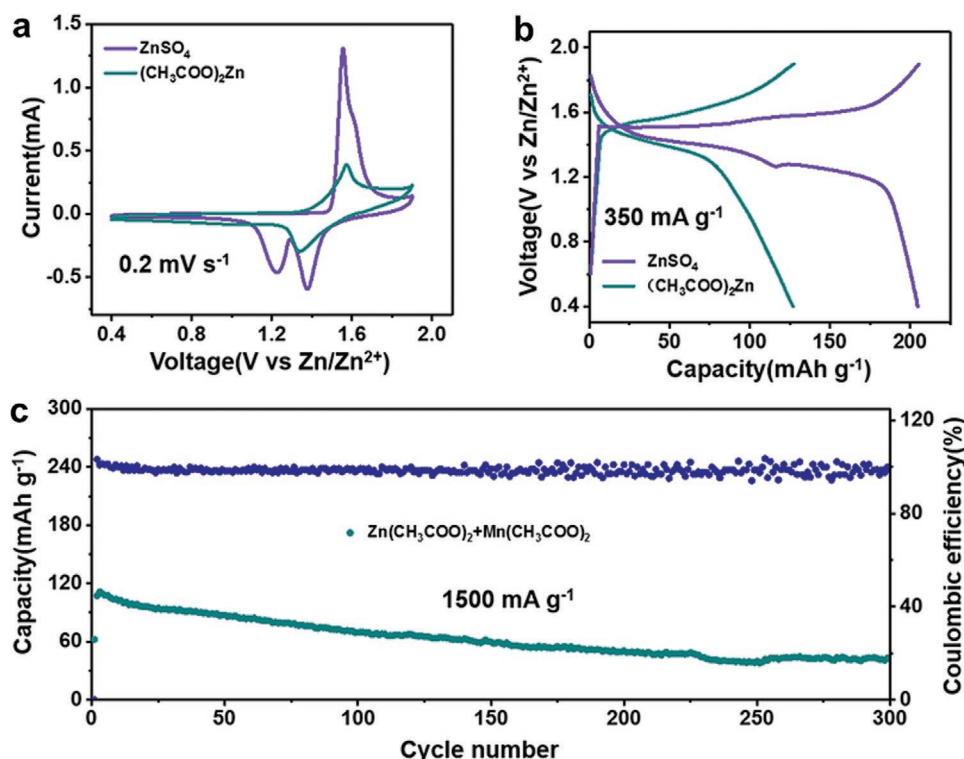


Figure 4. a) CV curves of CaMnO in ZnSO₄/MnSO₄ and Zn(CH₃COO)₂/Mn(CH₃COO)₂ electrolyte at 0.2 mV s⁻¹ (in the second cycle). b) Charge-discharge curves of CaMnO in 1 m ZnSO₄/0.1 m MnSO₄ and 1 m Zn(CH₃COO)₂/0.1 m Mn(CH₃COO)₂ electrolyte at 350 mA g⁻¹ (in the fifth cycle). c) Cycling stability of CaMnO in Zn(CH₃COO)₂/Mn(CH₃COO)₂ electrolyte at 1500 mA g⁻¹.

As displayed in Figure 3e, the CaMnO electrode achieves a discharge specific capacity of 100.9 mAh g⁻¹ after 5000 cycles at 3500 mA g⁻¹. The remarkable cycling life surpasses most of the previous reported aqueous ZIBs based on MnO₂ (Table S1, Supporting Information).

It is generally believed that the charge storage mechanism in the Zn//MnO₂ system is the cooperative insertion of H⁺ and Zn²⁺ ions in ZnSO₄/MnSO₄ electrolyte. However, it is unclear what factors affect the H⁺ ions' insertion, and the potential effect of the insertion of H⁺ ions on the electrochemical performance of Zn//MnO₂ system is uncertain. Thus, the electrochemical performances of CaMnO in different electrolytes are tested. The 1 m Zn(CH₃COO)₂/0.1 m Mn(CH₃COO)₂ electrolyte is used as control group due to its moderate pH (about 5.8), while 1 m ZnSO₄/0.1 m MnSO₄ electrolyte is mildly acidic (about 4.2). As shown in Figure 4a, the CaMnO electrode displays two discharge peaks in 1 m ZnSO₄/0.1 m MnSO₄ electrolyte, corresponding to H⁺ (1.4 V vs Zn/Zn²⁺) and Zn²⁺ (1.2 V vs Zn/Zn²⁺) ions insertion, respectively.^[13,21] It is worth noting that only one discharge peak at 1.3 V versus Zn/Zn²⁺ is discerned in 1 m Zn(CH₃COO)₂/0.1 m Mn(CH₃COO)₂ electrolyte, which may only be the insertion of Zn²⁺ ions.^[16] Simultaneously, the CaMnO electrode only has one discharge plat (Figure 4b) in 1 m Zn(CH₃COO)₂/0.1 m Mn(CH₃COO)₂ electrolyte, and the discharge specific capacity nearly reduces by half compared to 1 m ZnSO₄/0.1 m MnSO₄ electrolyte, only has 127 mAh g⁻¹. To further understanding whether the pH of electrolyte will affect the H⁺ ions insertion, we use CH₃COOH to adjust the pH of 1 m Zn(CH₃COO)₂/0.1 m Mn(CH₃COO)₂ electrolyte to

4.2. As shown in Figure S12a in the Supporting Information, the CV curves of CaMnO in Zn(CH₃COO)₂/Mn(CH₃COO)₂/CH₃COOH electrolyte display two discharge peaks in the previous three cycles. While the following cycle curve only has one peak, which may be due to the decrease of activity of hydrogen ions with complexation between H⁺ and CH₃COO⁻. Figure S12b in the Supporting Information indicates that the addition of H⁺ ions can improve the discharge specific capacity. The results indicate that the insertion of H⁺ ions is controlled by the pH of the electrolyte. Besides, the cycling life of CaMnO electrode in 1 m Zn(CH₃COO)₂/0.1 m Mn(CH₃COO)₂ electrolyte is tested at 1500 mA g⁻¹. As shown in Figure 4d, the CaMnO electrode achieves an initial discharge specific capacity of 107.3 mAh g⁻¹, and only has 39.4% capacity retention over 300 cycles in 1 m Zn(CH₃COO)₂/0.1 m Mn(CH₃COO)₂ electrolyte, while the CaMnO in 1 m ZnSO₄/0.1 m MnSO₄ electrolyte has high specific capacity and capacity retention (Figure 2d). The excellent electrochemical performance of CaMnO in 1 m ZnSO₄/0.1 m MnSO₄ electrolyte indicates that the H⁺ ions can improve the stability of CaMnO in first step of ions insertion, and benefits the Zn ions insertion into CaMnO in the following step, thus maintaining the long-term cycling life.

To further understanding the charge storage mechanism of CaMnO electrode, the XRD patterns of CaMnO electrode at the selected states are collected. As shown in Figure 5a, the typical ZnSO₄·3Zn(OH)₂·H₂O phase appears during the discharge processes, and gradually disappears during the charge processes, which suggests that H⁺ ions can reverse insertion/extraction.^[21] Note that, the CaSO₄·2H₂O phase is observed,

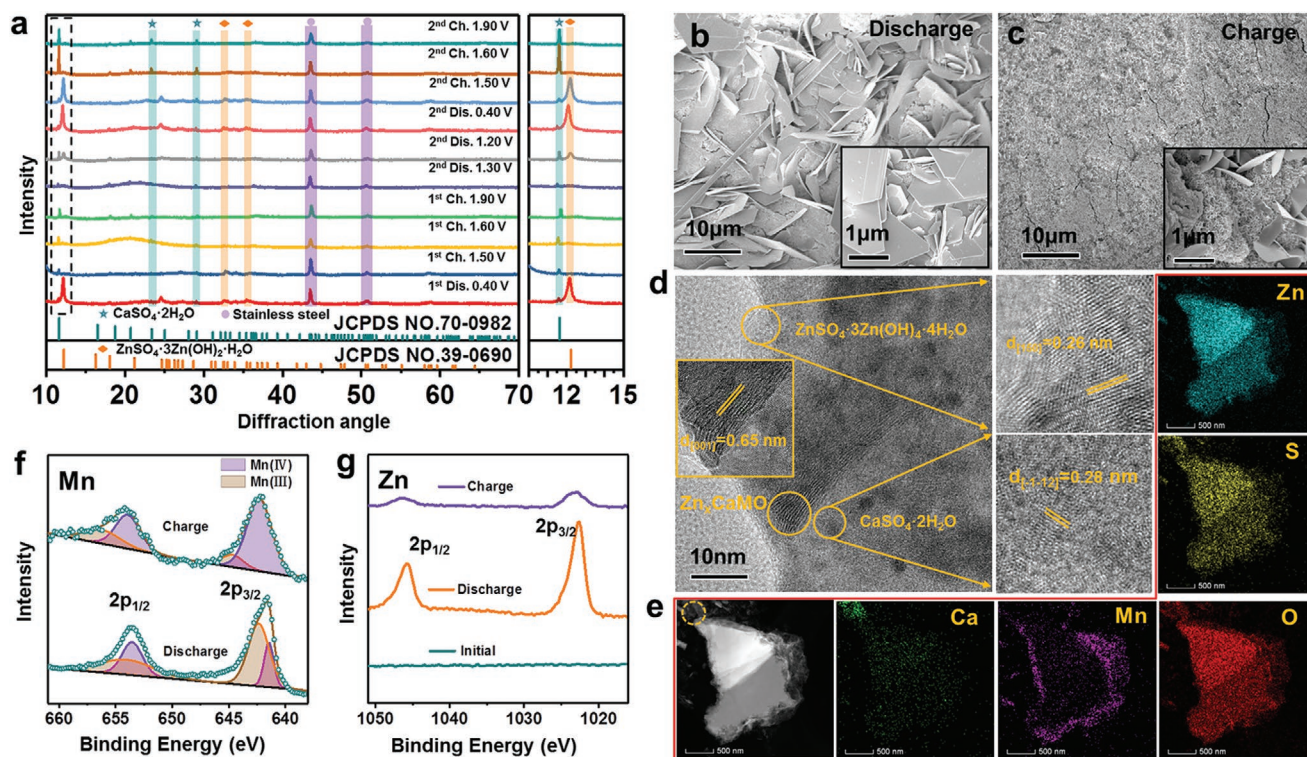


Figure 5. a) Ex situ XRD patterns of CaMnO during the first discharge and second charge/discharge cycle at 175 mA g^{-1} at different discharge and charge voltages. b,c) Ex situ SEM patterns of CaMnO, b) discharge to 0.4 V; c) charge to 1.9 V. d) HRTEM image of the CaMnO at discharged state (discharge to 0.4 V). e) STEM-EDS elemental mapping images of the CaMnO at discharged state (discharge to 0.4 V). f,g) The ex situ XPS spectra of Mn 2p and Zn 2p; f) Mn 2p; g) Zn 2p.

and is not disappeared during cycling processes. It may be due to the overcharging of initial cycle causing Ca^{2+} ions to precipitate from the CaMnO, then the Ca^{2+} ions form insoluble precipitate attaches to the CaMnO electrode surface. In addition, the (001) and (002) peaks of CaMnO phase are insignificant during the cycling processes. It is possible that the by-products on the surface of the electrode weaken the XRD intensity of CaMnO. Besides, the ex situ XRD of CaMnO in $1 \text{ M Zn}(\text{CH}_3\text{COO})_2/0.1 \text{ M Mn}(\text{CH}_3\text{COO})_2$ electrolyte is measured. As displayed in Figure S13 in the Supporting Information, the ZnMn_2O_4 (JCPDS No. 77-0470) phase exists in the discharge state, and disappears in charge state. Meanwhile, the CaMnO phase also is observed during the charge/discharge progress. The MnOOH phases are not detected in discharge state owing to without H^+ ions insertion. The ex situ SEM analysis further confirms the charge storage mechanism of CaMnO cathodes in different electrolytes. As shown in Figure 5b, the CaMnO electrode is covered by a layer of flake-like compounds at full discharge. Interestingly, some small-sized dispersed flake-like compounds are still present on the electrode surface (Figure 5c), which are the resulting $\text{CaSO}_4 \cdot 2\text{H}_2\text{O}$ precipitates during charge/discharge processes. The SEM elemental mapping in Figure S14 in the Supporting Information further confirms the results of XRD and SEM analysis. Moreover, no dendrites and by-product are found at Zn foil surface in either the charged or discharged state by SEM and XRD patterns (Figure S15a–d, Supporting Information), which suggests the excellent stability of Zn anode in $1 \text{ M ZnSO}_4/0.1 \text{ M MnSO}_4$

electrolyte. Meanwhile, we test the ex situ SEM of CaMnO electrode in $1 \text{ M Zn}(\text{CH}_3\text{COO})_2/0.1 \text{ M Mn}(\text{CH}_3\text{COO})_2$ electrolyte. As shown in Figure S16a,b in the Supporting Information, no flake-like compounds exist on the electrode surface at discharge state, which is consistent with the XRD results. The HRTEM analysis of CaMnO electrode at full discharge in $1 \text{ M ZnSO}_4/0.1 \text{ M MnSO}_4$ electrolyte is shown in Figure 5d. A lattice fringe with d -spacing of 0.65 nm is observed, corresponding to the (001) plane of CaMnO, which has hardly changed compared with the initial state (0.63 nm). According to the literature, the Zn^{2+} ions insertion will cause a lattice contraction due to the effect of interlayer electrostatic attraction and the expulsion of water from the interlayer, while the hydrated H^+ ions insertion will result in lattice expansion owing to the large hydration radius.^[22] The two opposite effects cancel each other out, and maintain constant layer spacing during the charge/discharge cycles. There are other two types of lattice fringes in the discharge products, corresponding to (150) $d = 0.26 \text{ nm}$ plane of $\text{ZnSO}_4 \cdot 3\text{Zn}(\text{OH})_2 \cdot \text{H}_2\text{O}$ and $(-1-12) d = 0.28 \text{ nm}$ plane of $\text{CaSO}_4 \cdot 2\text{H}_2\text{O}$, respectively. Furthermore, scanning transmission electron microscope (STEM)-EDS mapping analysis indicates that the discharge CaMnO cathode is composed of nanoflakes (CaMnO) and two sizes of flakes ($\text{ZnSO}_4 \cdot 3\text{Zn}(\text{OH})_2 \cdot \text{H}_2\text{O}$ and $\text{CaSO}_4 \cdot 2\text{H}_2\text{O}$). As shown in Figure 5e, the distribution elements in nanoflakes consist of Ca, Mn, O, and Zn, indicate that the Zn ions successfully insert into CaMnO. The bigger size of flake includes Zn, S, O elements and is without single Ca element, corresponding to $\text{ZnSO}_4 \cdot 3\text{Zn}(\text{OH})_2 \cdot \text{H}_2\text{O}$ flake. In contrast,

Ca, O, and S are uniformly distributed in the smaller flaky precipitate (the marked place with circle) with no signal of Zn, corresponding to $\text{CaSO}_4 \cdot 2\text{H}_2\text{O}$. The results of STEM-EDS mapping is evidenced by ex situ XRD and HRTEM. In addition, the HRTEM of full discharge CaMnO cathode in 1 M $\text{Zn}(\text{CH}_3\text{COO})_2/0.1$ M $\text{Mn}(\text{CH}_3\text{COO})_2$ electrolyte is shown in Figure S17 in the Supporting Information. The lattice fringes of CaMnO and ZnMn_2O_4 can be observed in the flake, which confirms that there is only Zn ions insertion in CaMnO electrode. Notably, the lattice spacing of (001) plane of CaMnO shrinks about 0.05 nm, which may originate only from the insertion of Zn ion. The STEM-EDS mapping (Figure S18, Supporting Information) shows the apparent signals of Ca, Mn, O, and Zn elements, which is consistent with the ex situ XRD analysis. The Nyquist plots for the CaMnO electrode in different electrolytes are obtained after five-cycle activation. As shown in Figure S19 in the Supporting Information, the charge transfer impedance of CaMnO in 1 M $\text{Zn}(\text{CH}_3\text{COO})_2/0.1$ M $\text{Mn}(\text{CH}_3\text{COO})_2$ electrolyte is much larger than that in 1 M $\text{ZnSO}_4/0.1$ M MnSO_4 electrolyte, which suggests that the Zn ions in 1 M $\text{ZnSO}_4/0.1$ M MnSO_4 electrolyte are more easily diffused into CaMnO cathode. Note that, the Nyquist plots of CaMnO in 1 M $\text{ZnSO}_4/0.1$ M MnSO_4 electrolyte have two semicircles as seen in the detailed image. The first semicircle may be corresponded to charge transfer impedance between the interface of electrolyte and $\text{CaSO}_4 \cdot 2\text{H}_2\text{O}$ precipitation on the electrode surface, and the second semicircle can be attributed to the interfacial charge transfer resistances between electrolyte and CaMnO electrode. To verify whether the $\text{CaSO}_4 \cdot 2\text{H}_2\text{O}$ precipitation has an effect on electrochemical performance of CaMnO , we design a set of controlled tests. The CaMnO cathode is disassembled from coin cell after five-cycle activation to produce enough $\text{CaSO}_4 \cdot 2\text{H}_2\text{O}$ precipitation on the electrode surface. Then the processed CaMnO electrode is reassembled to coin cell in 1 M $\text{Zn}(\text{CH}_3\text{COO})_2/0.1$ M $\text{Mn}(\text{CH}_3\text{COO})_2$ electrolyte. As shown in Figure S20 in the Supporting Information, compared to untreated electrode, both the specific discharge capacity and capacity retention of CaMnO have not improved. It suggests that the $\text{CaSO}_4 \cdot 2\text{H}_2\text{O}$ precipitation has no effect on the electrochemical performance of CaMnO electrode. We also investigate the evolution of Mn valence states during discharge/charge processes by XPS spectra. As shown in Figure 5f, the CaMnO includes great amount of Mn^{4+} in charge state, which significantly decrease in discharge state. The results indicate the decrease of Mn valence due to the intercalation of H^+ and Zn^{2+} during discharge processes. As shown in Figure 5g, two obvious peaks located at 1022 and 1045.1 eV are, respectively, attributed to Zn 2 $p_{3/2}$, and Zn 2 $p_{1/2}$ in discharge state, and the reduced amounts in the charged state suggest the reversible de-/insertion of Zn^{2+} ions. The cycling stability of CaMnO electrode in 1 M $\text{ZnSO}_4/0.1$ M MnSO_4 electrolyte is further confirmed by SEM patterns. Figure S21a–f in the Supporting Information shows the morphology evolution of CaMnO cathode during charge/discharge cycling. The morphology of CaMnO remains basically unchanged up to 5000 cycles, only the amount of nanoflakes is decreasing. Coincidentally, the capacity also begins to slightly drop from 4000th cycle (Figure 3e), accompanying the gradual disappearance of the hierarchical structure. Therefore, the per-intercalation of Ca ion and water in δMnO_2 can

enhance the structural stability and provide more cushion for relieving the strain generated from the Zn^{2+} and H^+ insertion/extraction.

3. Conclusion

In summary, we report a calcium ions and water-stabilized $\text{Ca}_{0.28}\text{MnO}_2 \cdot 0.5\text{H}_2\text{O}$ as cathode for aqueous ZIBs. We prove that the incorporation of hydrated calcium ion can intrinsically stabilize the layered structure of CaMnO cathode. Benefiting from this, the Zn// CaMnO battery achieves long cycling life over 5000 cycles with no obvious capacity fading, and excellent rate performance with a discharge specific capacity of 124.5 mAh g^{-1} at 3500 mA g^{-1} . Further, we explore both the factor and effect of H^+ insertion using different electrolytes. The H^+ diffusion is controlled by the pH and type of anion of electrolyte. Moreover, the insertion of H^+ in first step can stabilize the layer structure of cathode, and is in favor of the intercalation of Zn^{2+} in following step. Overall, the significant electrochemical performance of CaMnO makes the battery promising for future commercial ZIBs. Meanwhile, the strategy in this work to improve the performance of Mn-based material is expected to be general for many other battery material designs.

4. Experimental Section

Preparation of Electrode Materials: CaMnO was synthesized by hydrothermal method. CaCl_2 , KMnO_4 , and MnSO_4 with a molar ratio of 1:6:1 were dissolved in deionized water. The obtained solution was transferred into a 100 mL Teflon-lined stainless steel autoclave and maintained at 160°C for 12 h. Last, the product was centrifuged, washed with deionized water several times, and dried in a vacuum at 60°C for 12 h. δMnO_2 was synthesized with similar methods. Briefly, KMnO_4 and MnSO_4 were homogeneously mixed in deionized water with molar ratio of 6:1. Then the obtained solution was put into a Teflon-contained autoclave and heated at 160°C for 12 h. The resulting black precipitates were filtered, washed with deionized water several times, and then dried at 60°C in a vacuum overnight.

Characterizations: The crystallographic structure of the pristine materials was analyzed by XRD (Rigaku MiniFlex600 X-ray diffractometer with Cu K α). The morphologies and microstructures of the powders were examined by SEM (JEOL JSM-7500F) and HRTEM (FEI Talos F200XG2). XPS (PHI5000VersaProbe ESCALAB250xi) was used to characterize the intermediates at various charge/discharge states. The Raman spectra of CaMnO and δMnO_2 were tested by Raman spectroscopy (Thermo-Fisher Scientific, excitation from an argon-ion laser excitation wavelength, 532 nm). The structural water content in the as-prepared CaMnO cathode was measured by TGA from 30 to 800°C with a heating rate of $10^\circ\text{C min}^{-1}$ in Ar using a TG-DSC (thermogravimetry-differential scanning calorimetry) analyzer (NETZSCH, STA449F3). The molar ratio of Ca to Mn was measured using ICP-AES (ICAP 7400, Thermo).

Electrochemical Measurements: The CaMnO electrodes were prepared by mixing CaMnO , Ketjen black (KB), and polytetrafluoroethylene (PTFE) at an appropriate weight ratio of 8:1:1, and pressed onto stainless-steel mesh. Then the electrode films were dried at 80°C for 12 h under vacuum. The CaMnO mass loading was $1\text{--}2 \text{ mg cm}^{-2}$. The δMnO_2 electrodes were fabricated by pressing a mixture of a mass ratio of 80 wt% active material, 80 wt% KB, and 10 wt% PTFE onto a stainless-steel mesh and dried under vacuum at 80°C for 12 h. The δMnO_2 mass loading was $1\text{--}2 \text{ mg cm}^{-2}$. 1 M $\text{ZnSO}_4 + 0.1$ M MnSO_4 or 1 M $\text{Zn}(\text{CH}_3\text{COO})_2 + 0.1$ M $\text{Mn}(\text{CH}_3\text{COO})_2$ was used as electrolyte for full-cells test. CV and EIS were tested on Solartron 1400 electrochemical

workstation and charge/discharge was tested using Land-CT2001A battery instrument between a potential window of 0.4–1.9 V (vs Zn/Zn²⁺). The 2032-type coin cells were assembled by Zn foil as anode, CaMnO as cathode, glass fiber as separator, and standing about 10 h. Calculation of current density and specific capacity was based on the mass of CaMnO.

Supporting Information

Supporting Information is available from the Wiley Online Library or from the author.

Acknowledgements

This study was supported by the National Key R&D Program of China (2016YFB0901500); the National Natural Science Foundation of China (51771094, 21835004, and 21571148), Ministry of Education of China (B12015 and IRT13R30), and Tianjin Natural Science Foundation (no. 18JCZDJC31500).

Conflict of Interest

The authors declare no conflict of interest.

Keywords

aqueous zinc-ion batteries, birnessite, Ca_{0.28}MnO₂·0.5H₂O, cathode materials

Received: January 30, 2020

Revised: February 23, 2020

Published online:

- [1] a) Z. Guo, Y. Ma, X. Dong, J. Huang, Y. Wang, Y. Xia, *Angew. Chem., Int. Ed.* **2018**, 57, 11737; b) H. Y. Shi, Y. J. Ye, K. Liu, Y. Song, X. Sun, *Angew. Chem., Int. Ed.* **2018**, 57, 16359; c) F. Wan, L. Zhang, X. Wang, S. Bi, Z. Niu, J. Chen, *Adv. Funct. Mater.* **2018**, 28, 1804975; d) V. Soundharajan, B. Sambandam, S. Kim, V. Mathew, J. Jo, S. Kim, J. Lee, S. Islam, K. Kim, Y.-K. Sun, J. Kim, *ACS Energy Lett.* **2018**, 3, 1998.
- [2] a) V. Soundharajan, B. Sambandam, S. Kim, M. H. Alfaruqi, D. Y. Putro, J. Jo, S. Kim, V. Mathew, Y. K. Sun, J. Kim, *Nano Lett.* **2018**, 18, 2402; b) K. Zhu, T. Wu, K. Huang, *ACS Nano*. **2019**, 13, 1447; c) D. Chao, W. Zhou, C. Ye, Q. Zhang, Y. Chen, L. Gu, K. Davey, S. Z. Qiao, *Angew. Chem., Int. Ed.* **2019**, 58, 7823; d) N. Zhang, F. Cheng, J. Liu, L. Wang, X. Long, X. Liu, F. Li, J. Chen, *Nat. Commun.* **2017**, 8, 405; e) Q. Nian, J. Wang, S. Liu, T. Sun, S. Zhen, Y. Zhan, Z. Tao, J. Chen, *Angew. Chem., Int. Ed.* **2019**, 58, 16994.
- [3] a) J. Shin, D. S. Choi, H. J. Lee, Y. Jung, J. W. Choi, *Adv. Energy Mater.* **2019**, 9, 1900083; b) N. Zhang, M. Jia, Y. Dong, Y. Wang, J. Xu, Y. Liu, L. Jiao, F. Cheng, *Adv. Funct. Mater.* **2019**, 29, 1807331; c) L. Ma, S. Chen, C. Long, X. Li, Y. Zhao, Z. Liu, Z. Huang, B. Dong, J. A. Zapien, C. Zhi, *Adv. Energy Mater.* **2019**, 9, 1902446; d) L. Zhang, L. Chen, X. Zhou, Z. Liu, *Adv. Energy Mater.* **2015**, 5, 1400930; e) R. Trocoli, F. La Mantia, *ChemSusChem* **2015**, 8, 481; f) C. Guo, S. Tian, B. Chen, H. Liu, J. Li, *Mater. Lett.* **2020**, 262, 127180.
- [4] a) B. Wu, G. Zhang, M. Yan, T. Xiong, P. He, L. He, X. Xu, L. Mai, *Small* **2018**, 14, 1703850; b) M. Liu, Q. Zhao, H. Liu, J. Yang, X. Chen, L. Yang, Y. Cui, W. Huang, W. Zhao, A. Song, Y. Wang, S. Ding, Y. Song, G. Qian, H. Chen, F. Pan, *Nano Energy* **2019**, 64, 103942; c) H. Pan, J. F. Ellis, X. Li, Z. Nie, H. J. Chang, D. Reed, *ACS Appl. Mater. Interfaces* **2019**, 11, 37524; d) C. Yuan, Y. Zhang, Y. Pan, X. Liu, G. Wang, D. Cao, *Electrochim. Acta* **2014**, 116, 404; e) Y. Feng, Q. Zhang, S. Liu, J. Liu, Z. Tao, J. Chen, *J. Mater. Chem. A* **2019**, 7, 8122.
- [5] Y. Li, S. Wang, J. R. Salvador, J. Wu, B. Liu, W. Yang, J. Yang, W. Zhang, J. Liu, J. Yang, *Chem. Mater.* **2019**, 31, 2036.
- [6] M. H. Alfaruqi, J. Gim, S. Kim, J. Song, D. T. Pham, J. Jo, Z. Xiu, V. Mathew, J. Kim, *Electrochem. Commun.* **2015**, 60, 121.
- [7] D. Wang, L. Wang, G. Liang, H. Li, Z. Liu, Z. Tang, J. Liang, C. Zhi, *ACS Nano* **2019**, 13, 10643.
- [8] S. D. Han, S. Kim, D. Li, V. Petkov, H. D. Yoo, P. J. Phillips, H. Wang, J. J. Kim, K. L. More, B. Key, R. F. Klie, J. Cabana, V. R. Stamenkovic, T. T. Fister, N. M. Markovic, A. K. Burrell, S. Tepavcevic, J. T. Vaughey, *Chem. Mater.* **2017**, 29, 4874.
- [9] G. Fang, C. Zhu, M. Chen, J. Zhou, B. Tang, X. Cao, X. Zheng, A. Pan, S. Liang, *Adv. Funct. Mater.* **2019**, 29, 1808375.
- [10] H. Pan, Y. Shao, P. Yan, Y. Cheng, K. S. Han, Z. Nie, C. Wang, J. Yang, X. Li, P. Bhattacharya, K. T. Mueller, J. Liu, *Nat. Energy* **2016**, 1, 16039.
- [11] a) C. Xia, J. Guo, P. Li, X. Zhang, H. N. Alshareef, *Angew. Chem., Int. Ed.* **2018**, 57, 3943; b) P. Hu, T. Zhu, X. Wang, X. Wei, M. Yan, J. Li, W. Luo, W. Yang, W. Zhang, L. Zhou, Z. Zhou, L. Mai, *Nano Lett.* **2018**, 18, 1758; c) F. Ming, H. Liang, Y. Lei, S. Kandambeth, M. Eddaoudi, H. N. Alshareef, *ACS Energy Lett.* **2018**, 3, 2602; d) J. Wei, H. Ji, W. Guo, A. H. Nevidomskyy, D. Natelson, *Nat. Nanotechnol.* **2012**, 7, 357.
- [12] D. Kundu, B. D. Adams, V. Duffort, S. H. Vajargah, L. F. Nazar, *Nat. Energy* **2016**, 1, 16119.
- [13] W. Sun, F. Wang, S. Hou, C. Yang, X. Fan, Z. Ma, T. Gao, F. Han, R. Hu, M. Zhu, C. Wang, *J. Am. Chem. Soc.* **2017**, 139, 9775.
- [14] Y. Jin, L. Zou, L. Liu, M. H. Engelhard, R. L. Patel, Z. Nie, K. S. Han, Y. Shao, C. Wang, J. Zhu, H. Pan, J. Liu, *Adv. Mater.* **2019**, 31, 1900567.
- [15] S. Khamsanga, R. Pornprasertsuk, T. Yonezawa, A. A. Mohamad, S. Kheawhom, *Sci. Rep.* **2019**, 9, 8441.
- [16] C. Xu, B. Li, H. Du, F. Kang, *Angew. Chem., Int. Ed.* **2012**, 51, 933.
- [17] K. Zhu, T. Wu, K. Huang, *Adv. Energy Mater.* **2019**, 9, 1901968.
- [18] a) L. Zhao, J. Ni, H. Wang, L. Gao, *RSC Adv.* **2013**, 3, 6650; b) C. Julien, *Solid State Ionics* **2003**, 159, 345.
- [19] Z. Liu, Q. Yang, D. Wang, G. Liang, Y. Zhu, F. Mo, Z. Huang, X. Li, L. Ma, T. Tang, Z. Lu, C. Zhi, *Adv. Energy Mater.* **2019**, 9, 1902473.
- [20] C. Wang, D. Du, M. Song, Y. Wang, F. Li, *Adv. Energy Mater.* **2019**, 9, 1900022.
- [21] J. Huang, Z. Wang, M. Hou, X. Dong, Y. Liu, Y. Wang, Y. Xia, *Nat. Commun.* **2018**, 9, 2906.
- [22] L. Wang, K. Huang, J. Chen, J. Zheng, *Sci. Adv.* **2019**, 5, eaax4279.